Available online at www.sciencedirect.com
SCIENCE DIRECT®
European Journal of Mechanics B/Fluids 25 (2006) 164–171

Injection and coalescence of bubbles in a quiescent inviscid liquid ☆

F.J. Higuera *, A. Medina [1]

E. T. S. Ingenieros Aeronáuticos, Pza. Cardenal Cisneros 3, 28040 Madrid, Spain

Received 11 October 2004; received in revised form 17 March 2005; accepted 27 June 2005

Available online 1 September 2005

Abstract

Time periodic generation and coalescence of bubbles by injection of a gas at a constant flow rate through an orifice at the bottom of a quiescent inviscid liquid is investigated numerically using a potential flow formulation. The volume of the bubbles is determined for different values of a Weber number and a Bond number. Single bubbling and different regimes of coalescence are described by these computations. The numerical results show qualitative agreement with well-known experimental results for liquids of low viscosity, suggesting that bubble interaction and coalescence following gas injection is to a large extent an inviscid phenomenon for these liquids, many aspects of which can be accounted for without recourse to wake effects or other viscosity-dependent ingredients of some current models.

Keywords: Bubble generation; Coalescence; Potential flow

1. Introduction

The generation of bubbles by injection of a gas into a liquid at rest is an important and much studied problem. Extensive research has been summarized in a variety of models that address the many facets of the problem with different levels of detail; see Refs. [1–5] for reviews. The conceptually simplest models are based on a balance of the forces acting on a bubble of assumed shape (Refs. [6–8], among others). These models clearly show the existence of a regime of low gas flow rate in which the effect of the inertia of the liquid is negligible and the volume of the bubbles is a constant independent of the gas flow rate, and a regime of high gas flow rate in which the effect of the surface tension is negligible and the volume of the bubbles increases as the $6/5$ power of the gas flow rate and is independent of the size of the injection orifice.

The original models of Davidson and Schuler [6] and Ramakrishna et al. [7], which served to establish these results, have been extended to include a variety of effects such as the viscous drag of the bubbles, the flow left by the viscous wake of the preceding bubble, the momentum flux of the injected gas, and the different shapes and apparent masses of the bubble at different stages of its growth. Extensions also include a set of ad hoc criteria to account for the interference, collision and coalescence of bubbles [9], which are observed to occur at high flow rates and eventually

☆ This work was supported by the Spanish Ministerio de Ciencia y Tecnología under project DPI2002-4550-C07-5.
* Corresponding author.
E-mail address: higuera@tupi.dmt.upm.es (F. Higuera).
[1] On sabbatical leave from IMP, Mexico.

0997-7546/$ – see front matter
doi:10.1016/j.euromechflu.2005.06.001

lead to nonperiodic and chaotic regimes of bubble generation [10]. More sophisticated nonspherical models [11–15] postulate equations of motion for each element of the bubble surface, whose shape changes continuously during the growth and detachment. These models rely to varying degrees on solutions for the potential flow of the liquid [16]. Oguz and Prosperetti [17] numerically computed this flow using a boundary element method and described in full detail the growth and detachment of a single bubble at the end of a tube in different cases of interest, finding good agreement with high speed video visualizations (see also Ref. [18]).

This paper focuses on time periodic bubbling regimes featuring coalescence of two or more bubbles in a strictly inviscid liquid. Though the bubble generation process ceases to be periodic when the flow rate is increased to sufficiently high values, these more complex regimes will not be discussed here. Instead, the purpose of the work is to examine to what extent coalescence at moderate gas flow rates can be described in the framework of potential flow theory. In this respect, the work is an extension of those of Refs. [17] and [18] to include bubble coalescence. The main result is that potential flow computations suffice to describe many aspects of coalescence, without recourse to any wake effect or other effects related to the viscosity of the liquid.

Attention will be restricted to the simplest case of injection of a constant flow rate of a gas through a single circular orifice at the bottom of an inviscid liquid at rest. Fig. 1 is a sketch of the process. The gas will be treated as incompressible, with a density negligibly small compared with the density of the liquid. The only parameters of the problem are then the radius of the orifice, a, the density of the liquid, ρ, the liquid–gas surface tension and the contact angle of the surface with the bottom, σ and θ, the gas flow rate, Q (volume of gas injected per unit time), and the acceleration due to gravity, g. The dimensional parameters can be grouped into a Bond number and a Weber number

$$B = \frac{\rho g a^2}{\sigma} \quad \text{and} \quad We = \frac{\rho Q^2}{\sigma a^3}. \tag{1}$$

2. Formulation

The flow induced in the liquid by the train of bubbles issuing from the orifice of Fig. 1 is irrotational if the viscosity of the liquid is neglected. The velocity potential, φ such that $\boldsymbol{v} = \nabla\varphi$, satisfies the Laplace equation

$$\nabla^2\varphi = 0 \tag{2}$$

in the liquid, to be solved with the conditions

$$\frac{Df_i}{Dt} = 0, \tag{3}$$

$$\frac{D\varphi}{Dt} = \frac{1}{2}|\nabla\varphi|^2 - p_{g_i} - Bx + \nabla\cdot\boldsymbol{n}_i \tag{4}$$

at the surfaces of the bubbles; $\partial\varphi/\partial x = 0$ at the horizontal bottom ($x = 0$); and $\nabla\varphi \to 0$ at infinity. Here $f_i(\boldsymbol{x}, t) = 0$ is the equation of the surface of the i-th bubble, with $i = 0$ denoting the bubble growing at the orifice and $i = 1, 2, \ldots$ denoting the bubbles detached previously. These surfaces are to be found as part of the solution. Distances and times are nondimensionalized with the radius of the orifice a and the capillary time $(\rho a^3/\sigma)^{1/2}$. x is the dimensionless height above the bottom, $D/Dt = \partial/\partial t + \boldsymbol{v}\cdot\nabla$ is the material derivative at points of the bubble surfaces, $\boldsymbol{n}_i = \nabla f_i/|\nabla f_i|$, and p_{g_i} is the pressure of the gas in the i-th bubble referred to the pressure of the liquid at the bottom far from the orifice and scaled with σ/a. These pressures are functions of time which are determined by the conditions that the volume of the growing bubble ($i = 0$) increases at a constant rate equal to the volume of gas injected per unit time (Q), and the volumes of the detached bubbles ($i = 1, 2, \ldots$) do not change with time. In dimensionless variables, these conditions read

$$\int_{\Sigma_0} \boldsymbol{v}\cdot\boldsymbol{n}_0\,\mathrm{d}A = We^{1/2} \quad \text{and} \quad \int_{\Sigma_i} \boldsymbol{v}\cdot\boldsymbol{n}_i\,\mathrm{d}A = 0, \quad i = 1, 2, \ldots, \tag{5}$$

where the integrals extend to the surfaces of the bubbles.

An additional condition is needed at the contact line of the growing bubble with the solid. Here the contact line will be taken to coincide with the edge of the orifice when the angle of the liquid–gas surface with the horizontal is larger than the contact angle (i.e. when $-n_{x_0} < \cos\theta$, where n_{x_0} is the vertical component of the unit normal $\boldsymbol{n}_0$ to

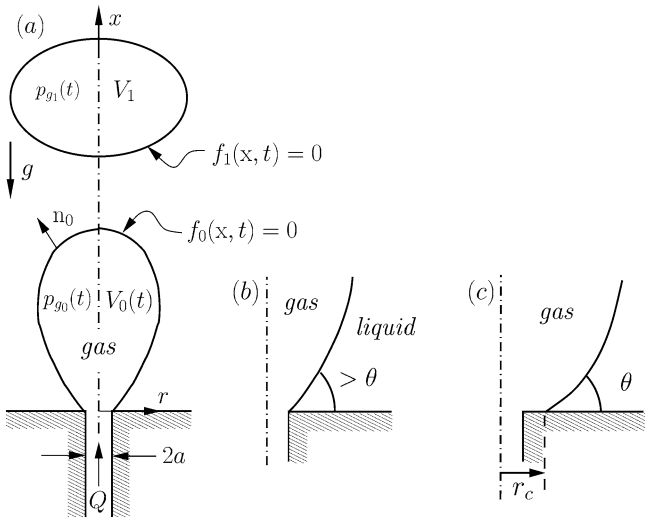

Fig. 1. Definition sketch, with details of the contact line attached to the edge of the orifice (b) and spreading on the horizontal bottom (c).

the attached bubble, see Fig. 1), and to spread away from the orifice with the liquid–gas surface making a constant contact angle with the solid ($-n_{x_0} = \cos\theta$) otherwise. The two possibilities are sketched in Figs. 1(b) and 1(c). The contact angle θ is a third parameter of the problem, along with B and We defined in (1).

Time periodic, axisymmetric solutions of the problem have been computed numerically using a standard boundary element method to solve the Laplace equation and a second order Runge–Kutta method to advance the material nodes at the surfaces of the bubbles and the velocity potential at them according to (3) and (4), with $p_{g_i}(t)$ determined to satisfy (5) at each time step. The implementation follows that of Oguz and Prosperetti [17]. In particular, cubic splines (for the known quantities) and six-point Gaussian quadrature are used to evaluate the contour integrals, and the nodes are redistributed at each time step to keep them equispaced. High frequency instabilities are smoothed by the procedure introduced by Oguz and Prosperetti [19], whereby a new set of nodes is generated at every time step by taking the mid points of the previous set. To reduce the computational burden, the number of bubbles simultaneously followed is limited to three by removing the uppermost bubble when a new bubble begins to grow at the orifice. Though this is a definite approximation, tests carried out keeping one more bubble have shown that the effect of the extra bubble on the growth and detachment of the bubble forming at the orifice, and on its possible coalescence with the bubble immediately above it, does not change the solution qualitatively.

An additional criterion is needed to handle the surface reconnections that occur at the detachment of a growing bubble, at the coalescence of two bubbles, and at the piercing of a bubble by a reentrant liquid jet (see below). Here a reconnection is assumed to occur when the distance between the two approaching surfaces becomes smaller than a certain cutoff of the order of the separation between the nodes used to discretize the surfaces. In typical computations, the number of nodes on the meridional section of each bubble ranges from 60 to 120 depending on the size of the bubble. The typical distance at which reconnection occurs is thus of the order of one hundredth of the size of the largest bubble involved in the process. Smoothing after reconnection is taken care of by the cubic splines used also in the rest of the computation [17].

3. Results and discussion

The purpose of the numerical results presented and discussed in this section is to show that the solution of the potential flow problem reproduces well-known features of the periodic generation and coalescence of bubbles in liquids of low viscosity; see, e.g., Refs. [3,9,10] and references therein. A numerical exploration of the full three-dimensional parameter space of the system has not been attempted. Such exploration would be very demanding, even with the simple numerical method described above, and probably not very rewarding, because the extensive experimental investigation of the problem carried out over many years makes unlikely that any new regime could be uncovered.

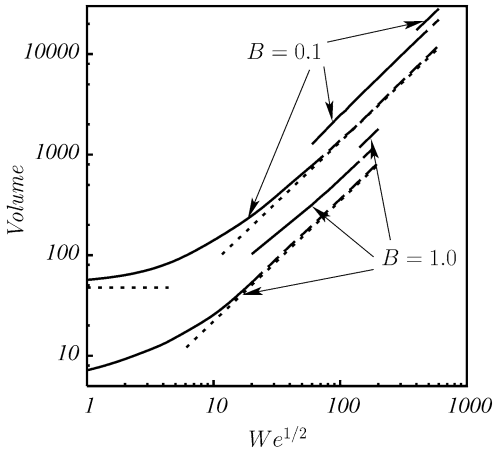

Fig. 2. Volume of the bubbles scaled with a^3 as a function of the dimensionless gas flow rate $We^{1/2}$ for $B = 0.1$ (upper set of curves) and $B = 1$ (lower set of curves). The solid curves of each set give the final volume of the bubble. The lower dashed curves give the volume of the first detached bubble of a compound bubble, and the intermediate dashed curves give the volume of the first detached couple when double coalescence occurs. The dotted horizontal line is the dimensionless volume 47.497 computed in [20] for quasi-static detachment at $B = 0.1$. For comparison, notice that the Fritz's dimensionless volume for $B = 0.1$ is $V_F = 2\pi/B = 62.83$. The dotted lines at the right correspond to volumes proportional to $We^{3/5}$.

The final volume of the bubbles is shown in Fig. 2 as a function of the dimensionless flow rate $We^{1/2}$ for two different values of the Bond number, $B = 0.1$ and $B = 1$, which correspond to orifices of radii $a = 0.85$ mm and 2.68 mm, respectively, in pure water. The contact angle was taken as $\theta = 45°$, though results for other values of θ are qualitatively similar.

The results for small $We^{1/2}$ show the well-known tendency of the bubble volume to become independent of the flow rate. In this range of small flow rates the bubbles grow quasi-statically and do not interact with each other. The final volume is the maximum volume for which surface tension and buoyancy forces can be in equilibrium [20]. For small values of the Bond number, the bubbles are nearly spherical and the dimensionless maximum volume is the Fritz volume $V_F = 2\pi/B$ [17,21].

The inertia of the liquid comes into play when the first term on the right hand-side of (4) becomes of the order of the buoyancy term Bx. Calling R the characteristic size of the bubble at detachment, the expansion of the bubble due to the (dimensionless) gas flow rate $We^{1/2}$ implies that $\nabla\varphi = \mathrm{O}(We^{1/2}/R^2)$ in the liquid around the bubble, and the inertia-buoyancy balance $|\nabla\varphi|^2 \sim BR$ requires $R \sim (We/B)^{1/5}$. Making here $R \sim V_F^{1/3}$ determines the flow rate at which the inertia of the liquid begins to matter as $We_c^{1/2} \sim 1/B^{1/3}$, while $V \sim R^3 \sim (We/B)^{3/5}$ for $We \gg We_c$ (see, e.g., Refs. [6] and [17]). This We_c determines the lower bound of the high flow rate regime mentioned above and gives also the order of the flow rate at which successive bubbles begin to interact. This is thus because the growth time of a bubble, $t_{\text{growth}} \sim R^3/We^{1/2} \sim We^{1/10}/B^{3/5}$, is of the order of the time t_{rise} it takes for the preceding bubble to rise a distance of the order of its size when We is of order We_c or larger (t_{rise} is obtained from the acceleration-buoyancy balance $R/t_{\text{rise}}^2 \sim B$, where the dimensionless apparent mass of the bubble is taken to be of order R^3).

What follows refers mostly to the numerical results for $B = 0.1$. Results for other values of the Bond number are similar. Identical bubbles grow and detach periodically at the orifice when $We^{1/2}$ is smaller than about 50. The mean distance between bubbles decreases when the Weber number increases, so that the growth of each bubble is increasingly affected by the bubbles above it. This regime is illustrated in Fig. 3. At all but very small Weber numbers, the volume of the bubbles at detachment is larger when the flow induced by the preceding bubbles is taken into account than when it is ignored, as it is done in single bubble computations.

The bubbles begin to couple in pairs when $We^{1/2}$ increases above 50. This regime has been also observed experimentally and was termed the pairing regime by Zhang and Shoji [9]. It is illustrated in Fig. 4 for $We^{1/2} = 100$. The leading bubble of each couple (labeled 1 in the figure) grows and detaches regularly. The trailing bubble (labeled 2) grows in the presence of the leading bubble and takes a prolate shape often noticed in the literature [3,9,10]. This prolate shape can be understood noticing that the leading bubble offers less resistance than the surrounding liquid to the flow induced by the expansion of the trailing bubble at the injection orifice, so that this expansion occurs preferentially upwards rather than horizontally. When the trailing bubble detaches, both bubbles rise together and approach

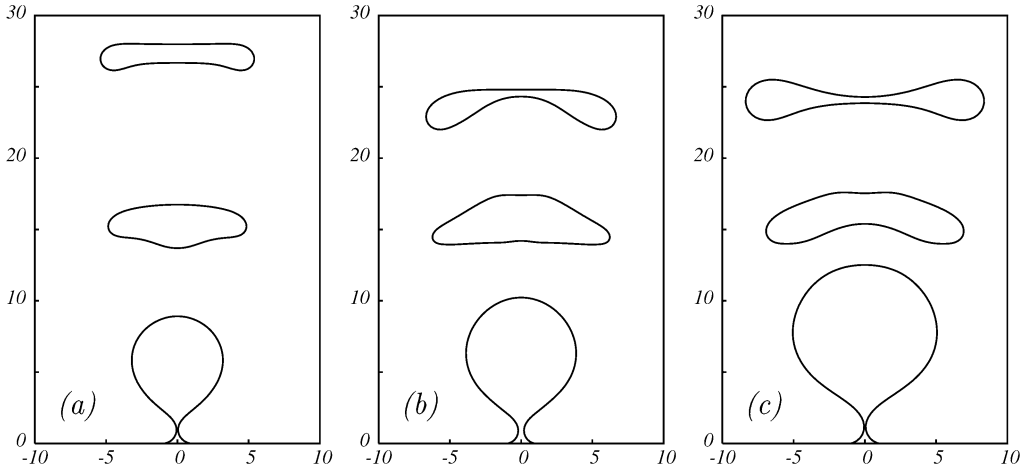

Fig. 3. Periodic generation of single bubbles for $B = 0.1$ and $We^{1/2} = 10$ (a), 20 (b), and 40 (c).

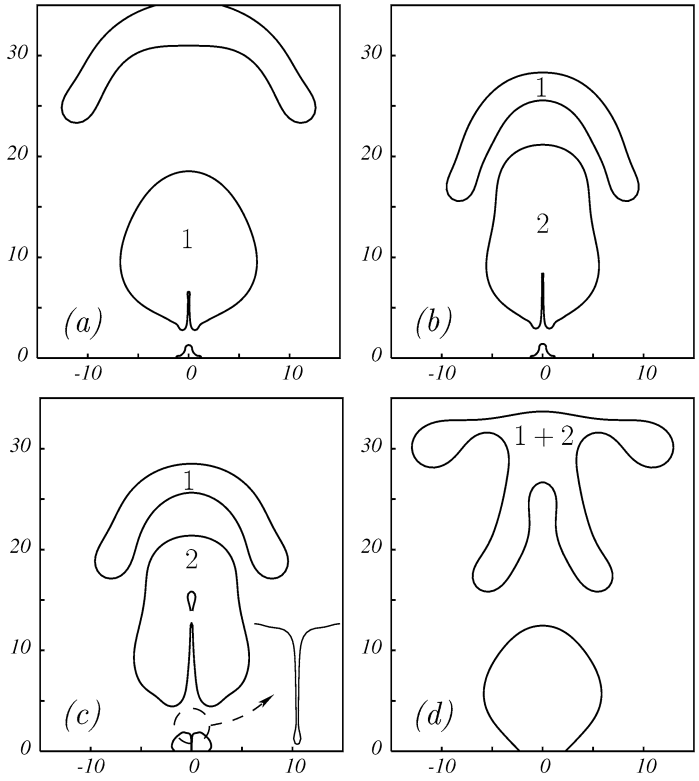

Fig. 4. Four snapshots of the generation of a (double) compound bubble for $B = 0.1$ and $We^{1/2} = 100$. (a) $t = 13.77$, immediately after the detachment of the leading bubble; (b) $t = 25.34$, immediately after the detachment of the trailing bubble; (c) $t = 25.64$, immediately after breakup of the thin upward jet; (d) $t = 33.68$, immediately after coalescence of the two bubbles. Times are nondimensionalized with the capillary time $(\rho a^3/\sigma)^{1/2}$ and measured from the detachment of the bubble preceding bubble 1 in (a). The period of the process is 25.34. Notice the weeping in (c) and the displacement of the contact line away from the orifice in (c) and (d).

each other until they eventually coalesce (bubble $1 + 2$). The coalescence of the detached bubbles is not always realized in real experiments [9] because non-axisymmetric perturbations may grow and put an end to the continuous approximation of the two bubbles.

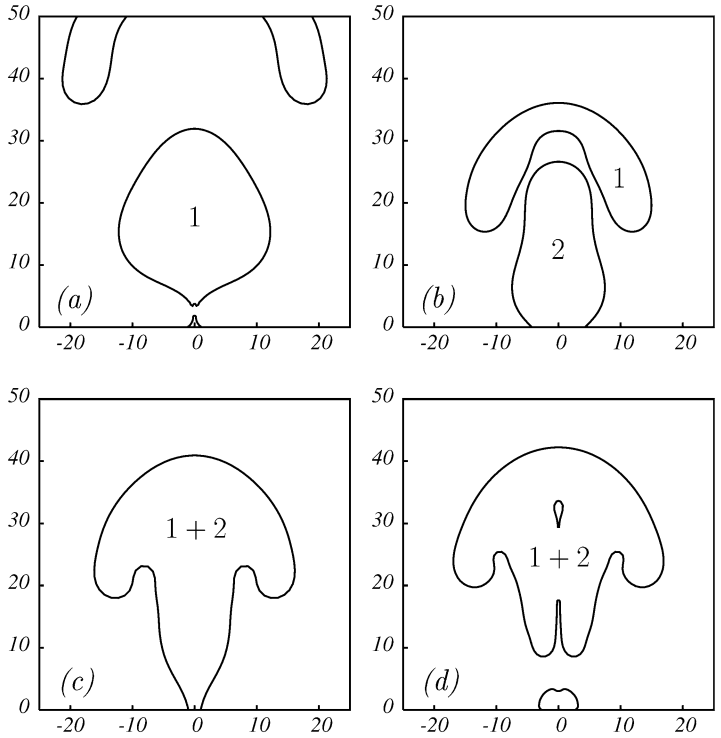

Fig. 5. Four snapshots of the generation of a (double) compound bubble for $B = 0.1$ and $We^{1/2} = 400$. (a) $t = 18.49$, immediately after the detachment of the leading bubble; (b) $t = 26.91$, during the growth of the trailing bubble; (c) $t = 30.79$, immediately after coalescence of the leading (detached) and trailing (attached) bubbles; (d) $t = 31.75$, immediately after detachment of the double bubble. The period of the process is 31.56.

The vertical elongation of the trailing bubble increases and the height of coalescence decreases when the Weber number is increased. As can be seen in Figs. 4(b) and 4(c), the upper part of the trailing bubble enters the concavity at the base of the leading bubble before the two bubbles coalesce. In lateral views, this may give the impression that the two bubbles have coalesced before they actually do.

Detachment of the trailing bubble and coalescence are almost simultaneous events in a wide range of Weber numbers. Coalescence precedes detachment of the trailing bubble above $We^{1/2} \approx 350$. This regime is illustrated in Fig. 5 for $We^{1/2} = 400$. The figure may be compared with Fig. 2c of Zhang and Shoji [9], for what these authors termed double coalescence regime. It has been observed in the numerical results that coalescence of two bubbles is always delayed by the velocity induced by the bubble immediately above the two bubbles that coalesce. Coalescence of a detached bubble and an attached bubble occurs at $We^{1/2}$ as low as 120 when that upper bubble is not present. This result shows the importance of the previously detached bubbles, which are only approximately represented in our three-bubble computations. The result may also have a bearing on the interpretation of the existing dispersion of experimental results (compare for example [9] and [10]), because three-dimensionality and possible breakdown (see below) limit the time interval during which a given bubble exerts its influence on the bubbles that follow it. In any case, the effect observed here is not due to the wake of the upper bubble, which is not accounted for in our irrotational flow computations.

Slightly above the value of $We^{1/2}$ for which the sequence detachment–detachment–coalescence changes to detachment–coalescence–detachment, the presence of the most recently formed double bubble affects the growth of the following bubble at the orifice sufficiently for this bubble to detach and rise without pairing with its successor. In the present axisymmetric computations the third bubble ends up coalescing with the double bubble to form a triple bubble. Again, this is not always the case in real experiments like those of Ref. [9] because the tridimensionality of the flow may prevent the second coalescence.

The height at which the second coalescence occurs decreases when the Weber number is further increased, but coalescence of a double bubble and a third bubble still attached to the orifice has not been observed numerically.

This result is at variance with the experiments of Zhang and Shoji [9], where such regime was observed and termed triple bubble formation. The discrepancy is to some extent a matter of detail, because coalescence into triple bubbles occurs in any case, but it may be pointing to an effect of the viscous drag of the double bubble. The drag, which is not accounted for here, would delay the rise of the double bubble and allow it to be reached by the following bubble growing at the orifice.

Results for other values of the Bond number are similar to the ones discussed above for $B = 0.1$. When the Bond number is increased, the bubbles become less spherical and detach earlier for a given value of *We*, and the detached bubbles very soon take a cap shape. Coalescence of detached bubbles begins to occur at $We^{1/2} \approx 20$ when $B = 1$, which is smaller than the corresponding dimensionless flow rate for $B = 0.1$ (see Fig. 2). The difference is in line with the estimates worked out above. Coalescence and detachment of the trailing bubble become almost simultaneous events above $We^{1/2} \approx 60$, and two successive coalescences leading to a triple bubble occur above $We^{1/2} \approx 150$.

Breakup of the neck joining the bubble to the orifice is always followed by retraction of the surface and formation of a thin and very fast reentrant jet that shoots across the detached bubble. The tip of the jet breaks into one or a few tiny drops that hit the ceiling of the bubble (see, e.g., Figs. 4(a)–(c) and 5(d)). These drops can be observed in high speed video visualizations like that of Fig. 6, in which appropriate illumination allows to see through recently detached bubbles. The motion of the drops inside the bubble and their subsequent impact on the ceiling of the bubble have not been followed in detail numerically. Instead, the drops have been suppressed when the jet breaks up, and their mass and a fraction of their vertical momentum have been instantaneously added to the liquid around the uppermost point of the bubble surface. Numerical tests show that the solution does not change much if the mass and momentum of these small drops are ignored.

The retraction of the surface immediately after pinchoff is an effect of both the surface tension [22] and the overpressure which appears in the liquid around the breakup point to stop the radially inward flow induced earlier by the collapse of the neck. These forces act on the base of the detached bubble, originating the upward moving jet discussed above, and on the upper surface of the new bubble growing at the orifice, which undergoes one or two oscillations. In some cases these oscillations develop into a downward moving jet which enters the injection orifice (as in Fig. 4(c); see also [23] and references therein). In the present computations, this phenomenon of weeping has been observed in narrow ranges of the flow rate around $We^{1/2} = 100$ and 400 for $B = 0.1$ and around $We^{1/2} = 40$ for $B = 1$.

The thin upward moving jet is followed by a thicker jet when the Weber number is sufficiently high. This thick jet originates at the concave base of the most recently detached bubble and may develop and pierce the bubble before being strangled by the coalescence of a new bubble at its base. The result is a toroidal bubble, which is unstable to non-axisymmetric perturbations and rapidly breaks down [3]. The computations have been stopped when a jet hits the ceiling of the most recently detached bubble.

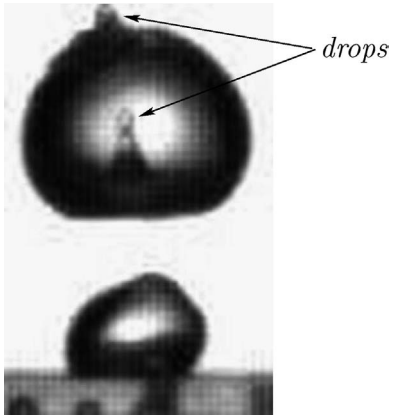

Fig. 6. Image from a high speed video showing a small drop breaking off the reentrant jet at the base of a recently detached bubble and another drop that has already crossed the bubble and is impacting on its upper surface. The asymmetry of the bubble and the jet is due to a small irregularity of the injection orifice. The orifice radius and gas flow rate are $a = 0.5$ mm and $Q = 35$ lit/h, leading to $B = 0.03$ and $We = 1.04 \times 10^4$ if the surface tension of pure water is assumed.

Three or more consecutive coalescences, leading to compound bubbles made of four or more elements, have been reported in [9] and [10], for example, but have not been observed numerically before the solution ceases to be periodic for the reason discussed in the preceding paragraph.

4. Conclusions

Numerical computations have been carried out of the axisymmetric, irrotational, time periodic flow induced in a quiescent strictly inviscid liquid by the growth, detachment and coalescence of bubbles due to the injection of a constant gas flow rate through a horizontal submerged orifice. The results show that this simple potential flow formulation may qualitatively describe many aspects of the well-known transition from quasi-static generation of independent, constant volume bubbles at low Weber numbers to inertia and buoyancy controlled growth and interaction of bubbles at moderately high Weber numbers. The simple computations presented here reproduce the single and double coalescences that occur when the Weber number is increased, and that lead to compound bubbles. A vigorous reentrant jet is seen to cross the compound bubble and impact on its ceiling when the Weber number is high, probably causing the breakdown of the bubble and marking the end of the regime of periodic bubble generation. The critical Weber number at which coalescence first occurs decreases when the Bond number is increased. Other experimentally observed phenomena, such as tiny drops shooting across the bubbles, weeping, and the motion of the contact line away from the orifice are also observed in these computations.

References

[1] R. Kumar, N.R. Kuloor, The formation of bubbles and drops, Adv. Chem. Engrg. 8 (1970) 255.
[2] R. Clift, J.R. Grace, M.E. Weber, Bubbles, Drops, and Particles, Academic, New York, 1978.
[3] N. Räbiger, A. Vogelpohl, Bubble formation and its movement in Newtonian and non-Newtonian liquids, in: N.P. Cheremisinoff (Ed.), Encyclopedia of Fluid Mechanics, vol. 3, Gulf Publishing Company, Houston, 1986 (Chapter 4).
[4] H. Tsuge, Hydrodynamics of bubble formation from submerged orifices, in: N.P. Cheremisinoff (Ed.), Encyclopedia of Fluid Mechanics, vol. 3, Gulf Publishing Company, Houston, 1986 (Chapter 9).
[5] S.S. Sadhal, P.S. Ayyaswamy, J.N. Chung, Transport Phenomena with Drops and Bubbles, Springer, 1997 (Chapter 7).
[6] J.F. Davidson, B.O.G. Schuler, Bubble formation at an orifice in an inviscid liquid, Trans. Inst. Chem. Engrg. 38 (1960) 335.
[7] S. Ramakrishna, R. Kumar, N.R. Kuloor, Studies in bubble formation – I: Bubble formation under constant flow conditions, Chem. Engrg. Sci. 24 (1968) 731.
[8] S.C. Chuang, V.W. Goldschmidt, Bubble formation due to a submerged capillary tube in quiescent and coflowing streams, ASME J. Basic Engrg. 92 (1970) 705.
[9] L. Zhang, M. Shoji, Aperiodic bubble formation from a submerged orifice, Chem. Engrg. Sci. 56 (2001) 5371.
[10] T.G. Leighton, K.J. Fagan, J.E. Field, Acoustic and photographic studies of injected bubbles, Eur. J. Phys. 12 (1991) 77.
[11] A. Marmur, E. Rubin, A theoretical model for bubble formation at an orifice submerged in an inviscid liquid, Chem. Engrg. Sci. 31 (1976) 453.
[12] W.V. Pinczewski, The formation and growth of bubbles at a submerged orifice, Chem. Engrg. Sci. 36 (1981) 453.
[13] R.B.H. Tan, I.J. Harris, A model for non-spherical bubble growth at a single orifice, Chem. Engrg. Sci. 41 (1986) 3175.
[14] J.-L. Liow, N.B. Gray, A model of bubble growth in wetting and non-wetting liquids, Chem. Engrg. Sci. 43 (1988) 3129.
[15] K. Terasaka, H. Tsuge, Bubble formation under constant-flow conditions, Chem. Engrg. Sci. 48 (1993) 3417.
[16] A.E. Wraith, T. Kakutani, The pressure beneath a growing rising bubble, Chem. Engrg. Sci. 29 (1974) 1.
[17] H.N. Oguz, A. Prosperetti, Dynamics of bubble growth and detachment from a needle, J. Fluid Mech. 257 (1993) 111.
[18] H.N. Oguz, J. Zeng, Axisymmetric and three-dimensional boundary integral simulations of bubble growth from an underwater orifice, Eng. Anal. Boundary Elements 19 (1997) 319.
[19] H.N. Oguz, A. Prosperetti, Bubble entrainment by the impact of drops on liquid surfaces, J. Fluid Mech. 219 (1990) 143.
[20] M.S. Longuet-Higgins, B.R. Kerman, K. Lunde, The release of air bubbles from an underwater nozzle, J. Fluid Mech. 230 (1991) 365.
[21] W. Fritz, Berechnung des maximalen Volumens von Dampfblasen, Phys. Z. 36 (1935) 379.
[22] D. Leppinen, J.R. Lister, Capillary pinch-off in inviscid fluids, Phys. Fluids 15 (2003) 568.
[23] W. Zhang, R.B.H. Tan, A model for bubble formation and weeping at a submerged orifice, Chem. Engrg. Sci. 55 (2000) 6243.